Computational Analysis of Impulse Forces Affecting Coil Compaction in Cerebral Aneurysms

Kyung Se Cha, Elias Balaras

Department of Mechanical Engineering, University of Maryland, College Park, MD, USA

Abstract

The effectiveness of the treatment of intracranial aneurysms with endovascular coiling depends on coil packing density, the location of aneurysm, its neck dimensions with respect to the aneurysm dome, and its size with respect to the surrounding tissue. Clinical data also suggests that the aneurysm neck size is the main predictor of aneurysm recanalization. In this study, the force impinging on the aneurysm neck in an idealized aneurysm was calculated by using a three dimensional finite volume method for the non-Newtonian incompressible laminar flow. To quantify the effect of neck size on the impingement force, calculations were performed for aneurysm neck diameters (Da) varying from 10% to 100% of the parent artery diameter (Dp). Also, maximum impingement forces were represented by a function of the ratio of the aneurysm neck to the diameter of the parent vessel. The results show that the hemodynamic forces exerted on the coil mass at the aneurysm neck due to the pulsatile blood flow are larger for wide necked aneurysms.

Key words : intracranial aneurysm, hemodynamics, non-newtonian fluid, coil compaction

I . INTRODUCTION

A neurysms in cerebral arteries, which are usually in the shape of a pouch or balloon, are caused by the weakness of the arterial wall. These aneurysms occur mostly in curved arteries and at arterial bifurcations [1], [2]. Rupture of these aneurysms is the leading cause of subarachnoid hemorrhage, which has high mortality and morbidity rate [3],[4].

To treat aneurysms, surgical and endovascular techniques are considered [5]. Surgical clipping consists of placing a clip across the neck of the aneurysm in order to block blood flow into the aneurysm. Because of the difficulties and high risks associated with these surgical procedures, the treatment of aneurysms with endovascular coiling is preferred over surgical clipping [6-8]. In the early 1990s, an endovascular technique became available in which detachable coils were inserted inside the aneurysm sac. At first, this endovascular treatment was limited to aneurysms which were difficult to treat surgically. However, recently, this treatment has become widespread and can also be applied to aneurysm which could be treated surgically. Using the endovascular techniques, detachable coils are inserted into the aneurysm sac, which

Corresponding Author : Kyung-Se Cha
2181 Glenn L. Martin Hall, University of Maryland, College Park, MD 20742, USA.
Tel : +1-301-792-6748 / Fax : +1-301-314-9477
E-mail : chaks@umd.edu

reduce the local flow in the aneurysm sac sufficiently and rupture can be then prevented by the thrombus formation.

Risk factors for failure of aneurysm coiling treatment have been identified as low coil packing density, location of the aneurysm, its neck dimensions with respect to the aneurysm dome, and its size with respect to the surrounding tissue. Clinical data also suggests that neck size appears to be the main predictor for recanalization [9]. Currently, the coil-packing density of the aneurysm volume that is usually achieved is about 35% or less. Thus, coil compaction and aneurysm recanalization remain a major long-term risk.

Flow characteristics following coil embolization have been investigated in vivo and vitro studies [10], [11]. Groden et al. [12], Lieber and Gounis [13] have applied computational fluid dynamics (CFD) to the idealized flow geometries of stented and coiled blood vessel with aneurysm. Recently, Liang-Der Jou et al. [14] applied computational fluid dynamic approaches to determine the pressure and shear stresses on the fusiform aneurysm wall. They used MR angiography to determine aneurysm geometry and MR velocimetry to quantify velocity fields. Lieber et al. [15] evaluated the maximum force impinging on the aneurysm neck in a simplified aneurysm geometry using the impulse momentum equation and Womersley's flow.

Byun et al. [16] analyzed the velocity fields using the computational fluid dynamics in lateral aneurysm models, which were partially blocked by coils, and investigated the flow changes for different coil locations. They also observed

the effects of parent vessel curvature. Gordan et al. [17]presented the methodology which can be applicable in the simulation of endovascular aneurysm treatment using the finite element method.

Lieber et al. [15] hypothesized that the forces exerted by direct and repeated impingement of the pulsatile blood flow in the coil are larger for wide necked aneurysms and may be responsible for their compaction and aneurysm recanalization. To verify this hypothesis they evaluated the maximum force impinging on the coils in an idealized coiled aneurysm placed at the apex of the bifurcation using a control-volume integral formulation.

As an extension of the study presented in Lieber et al. [15], the pulsatile flow in idealized bifurcation aneurysms treated with coils was calculated using a fully three-dimensional finite volume method for incompressible flows. The main objective of the present study is the analysis of the hemodynamic forces affecting coil compaction in cerebral aneurysms. In the following pages, the computational methods and results will be described in detail.

II. NUMERICAL METHODS

The three-dimensional, incompressible, laminar flow has been calculated using the finite volume method. The numerical scheme is a second order which is accurate in both space and time. The fluid flow is modeled with the Navier-Stokes equations which contain the conditions of the conservation of mass and momentum. These equations can be written as the continuity equation.

$$\frac{\partial u_k}{\partial x_k} = 0 \qquad (1)$$

the momentum equation.

$$\rho \frac{\partial u_j}{\partial t} + \rho u_k \frac{\partial u_j}{\partial x_k} = -\frac{\partial p}{\partial x_j} + \mu_e \frac{\partial^2 u_j}{\partial x_i^2} \qquad (2)$$

where u_j is the fluid velocity vector, ρ is the density, p is the pressure and μ_e represents the viscosity of the blood.

The rheological behavior of blood is approximated using a shear-thinning model. In the present study, the Carreau model [18] was employed to account for the non-Newtonian, shear thinning nature of blood:

$$\mu_e = \mu_\infty + (\mu_0 - \mu_\infty)[1 + (\lambda \dot\gamma)^2]^{\frac{n-1}{2}} \qquad (3)$$

where μ_0, μ_∞ and λ and n are the viscosity at zero shear,

viscosity at infinite shear, a time constant and the flow behavior index. The shear rate, $\dot\gamma$, was defined as

$$\dot\gamma = \sqrt{2tr(D^2)} \qquad (4)$$

where $D = [\nabla u + (\nabla u)^T]/2$ is the rate of deformation tensor. Parameters in Eq. (3) are expressed as $\mu_0 = 0.01072 Pa \cdot s$, $\mu_\infty = 0.00066028 Pa \cdot s$, $\lambda = 2.6504s$ and $n = 0.3568$.

III. NUMERICAL RESULTS

A. Pulsatile Flow through a Constricted Tube

The pulsatile flow through a constricted (45% area reduction) tube was considered to verify the present numerical algorithm for the periodic fluid flow. As shown in Fig. 1, the 45% (by area, or 25.84% by diameter) axisymmetric stenosis was used in the simulation. The fluid was assumed to be incompressible and Newtonian, and the wall was rigid in this case. Pulsatile flow was specified at the inlet as a sinusoidal volumetric flow waveform of 4.3 ± 2.6 ml with a period of 345 ms, based on the experiment by Ojha et al. [19]. The fluid had a density of 755 kg/m^3 and a viscosity of 0.00143 Ns/m^2. The mean Reynolds number (Re) of the flow was 575, and the modulation Reynolds number was 360. In other words, the maximum and minimum Reynolds numbers are 935 and 215 respectively. Since the Re was less than 2000 during the cycle and the stenosis was mild, it was reasonable to treat the flow as laminar. A frequency parameter of 7.5: values that are similar to those found in the human internal carotid artery. The inlet boundary condition was assumed by fully developed axial velocity profiles calculated from the time-dependent flow rate.

The numerical model of flow alone was validated with the experimental data obtained by Ojha et al. [19], at three different locations in the post-stenotic region Z = 1, Z = 2.5
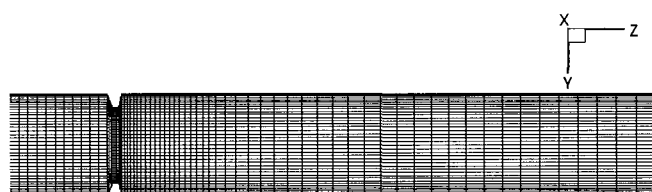

Fig. 1. Geometry of stenosed tube
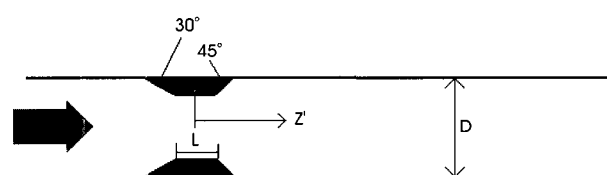

Fig. 2. Grid system of pulsating flow through a constricted tube

and Z = 4.3, where Z is the normalized distance from the center of the stenosis, i.e. Z = Z'/D, Z' is the axial distance away from the center of the stenosis and D is the inlet diameter of the tube (Fig. 1). As shown in Fig. 2, the 3-dimensional meshes contain 58719 nodes and 53240 elements for this problem. The flow waveform specified at the model inlet was identical to that in the experiment of Ojha et al. [19], as shown in Fig. 3.
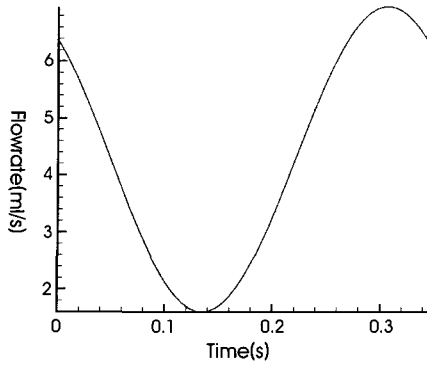

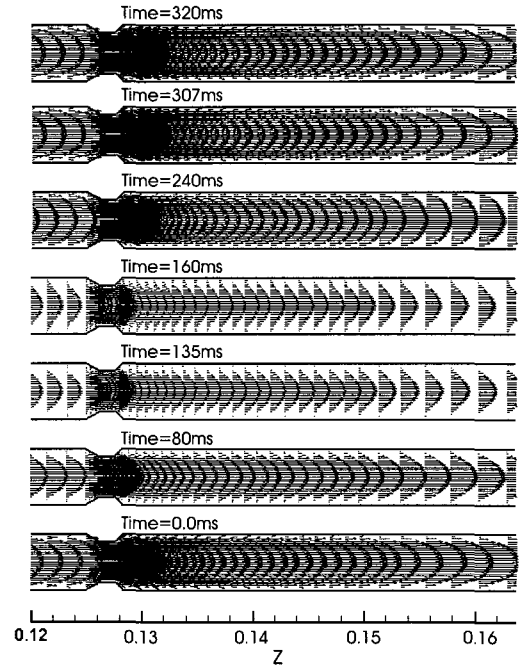Fig. 3. The volumetric waveform used in the simulation

Fig. 4. Selected velocity vectors at the indicated times through the flow cycle for the 45% axisymmetric stenosis.
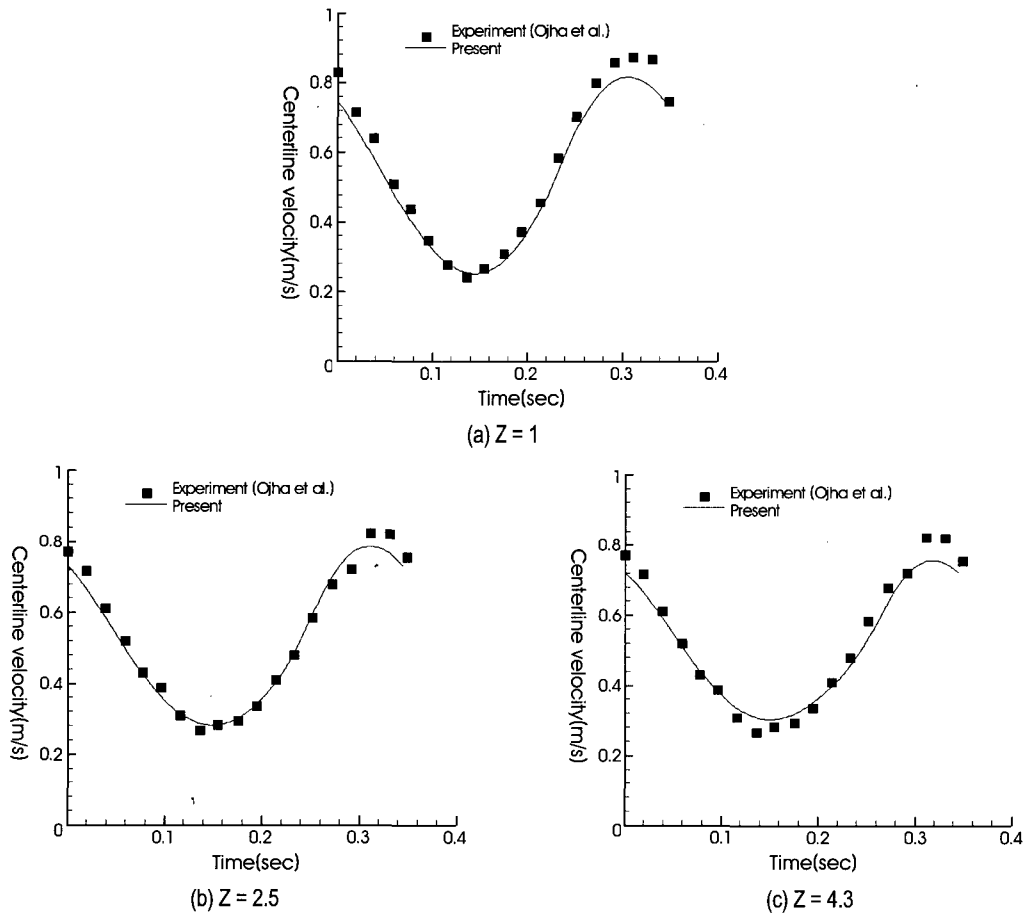

(a) Z = 1

(b) Z = 2.5

(c) Z = 4.3

Fig. 5. Comparison of centerline axial velocity between predictions and measurements of Ojha et al. [19]at normalized post-stenotic distance of Z = 1, 2.5 and 4.3.

Figure 4shows selected velocity vectors at the indicated times through the flow cycle for the 45% axisymmetric stenosis. The period is 345 ms and the times $T_{min} = 135$, and $T_{max} = 307$ are the instants of minimum and maximum flow. The centerline velocities predicted from the simulation were compared with the measurements as shown in Fig. 5. The present results are in agreement with experimental data [19].

B. The Blood Flow in a Micro-Tube

The numerical algorithm for non-Newtonian fluid was validated by predicting the blood flow in a micro-tube. The calculation was accomplished for the case where D=$90\mu m$, $\rho = 1050 Kg/m^3$, and Re = 0.107. A schematic view of the geometry and dimensions is shown in Fig. 6. In this numerical simulation, the blood flow was predicted using the Carreau model [18]. In previous research, Hernan and Gonzalez [20] also calculated this problem using the Casson model. Figure 7 shows the dimensionless velocities calculated for a Carreau fluid, a Casson fluid and the experimental data for blood flow measured by Einav et al. [21].

The velocity profiles show a plug type of flow which is the evidence of the non-Newtonian behavior of this fluid. Also, the results presented in Fig. 7 are in good agreement with the experimental results of Einav et al. [21].
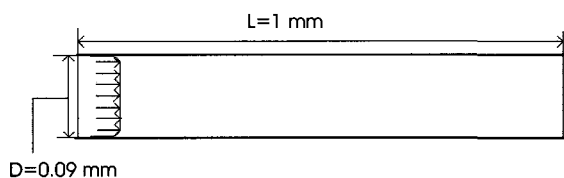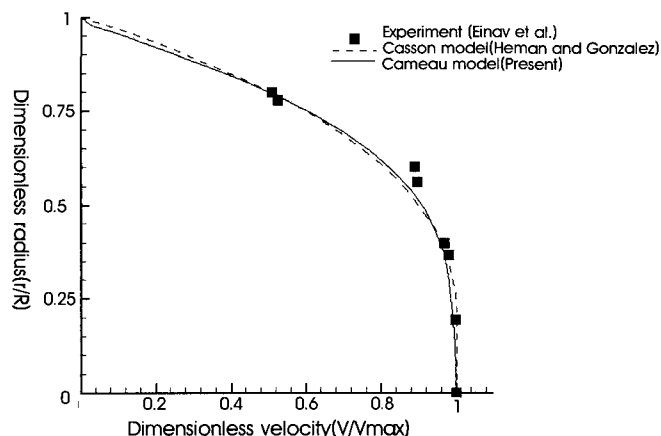
C. Pulsatile Flow in Idealized Coiled Aneurysm

The three-dimensional pulsatile flow in idealized models of coiled cerebral aneurysms was calculated as shown in Fig. 8. The mesh for this problem is shown in Fig. 9. Since the aneurysm was assumed to be filled with coils, there was no flow in the interior of the aneurysm. To investigate the effects of the neck size on the impingement force, calculations were performed for aneurysm neck diameter (Da) varing from 10 % to 100 % of the parent artery (Dp). Each daughter branch has half the cross sectional area of the parent artery. Fig. 10 shows the pulsatile flow waveform at the inflow region. The temporal variation in the mean blood flow through the parent artery over one cardiac cycle was obtained from previous research [22]. Based on this waveform, the time varying analytical solution for fully developed pulsatile flow in a pipe was computed and imposed at the inflow plane as a boundary condition. The maximum and mean Reynolds numbers, based on parent artery diameter and flow rates, were 474 and 387 respectively. In these computations, blood was considered a non-Newtonian fluid with a density of 1100 kg/m^3 and a viscosity of 0.0035 Pa s. The artery wall was assumed to be rigid.

L=1 mm

D=0.09 mm

Fig. 6. Schematic of the geometry and dimension for the flow of a non-Newtonian fluid.

Fig. 7. Velocity profiles at the outlet

Filled with coils

Da

Fz

Dc=2.546mm

Outflow

Outflow

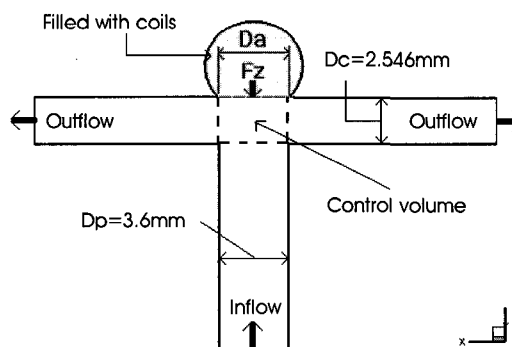Dp=3.6mm

Control volume

Inflow

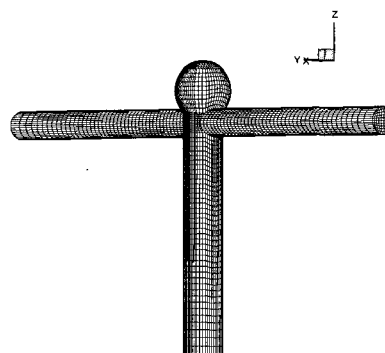Fig. 8. Schematic of the geometry for the idealized aneurysm

Fig. 9. The mesh for the idealized aneurysm

In this computation, four cycles were required for the flow to reach a periodic steady state and become independent of the initial conditions. Figure 11 shows the normal velocity component at three different phases of a flow cycle which affects the force on the coiled aneurysm neck. The calculated maximum peak velocity through the parent artery was 0.838 m/s. As the flow is accelerated, upward flow impinges strongly on the aneurysm neck. And then, at the bifurcation, the flow is redirected into the daughter vessels resulting in a force being exerted on the aneurysm neck. The forces on the virtual coil, represented by the surface shown in Fig. 8, were computed during each cardiac cycle. To evaluate the forces, the impulse-momentum equation for fluid flow was used. Using this law, the forces exerted on the coil mass at the neck of a basilar top aneurysm was expressed by the change in momentum of the fluid carried within control volume.
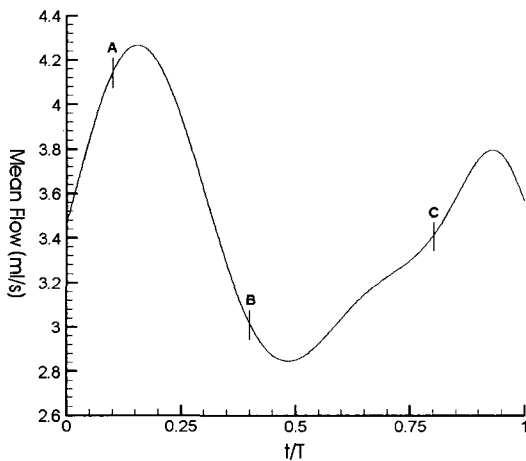
Fig. 10. Mean flow waveform at the inlet of a parent vessel during a flow cycle.

To investigate the dependency the computational mesh, we conducted simulations on three different grid systems (Grid I, II and III). The grid resolution was gradually increased by approximately 50%. In all cases grid points were clustered in areas of large velocity gradients that were illuminated by the coarser simulations. Grid I, II and III had approximately 42200, 65700, 95300 nodes respectively. In Fig. 12, the forces during the pulsatile cycle are shown for the case where Da = Dp. It can be seen that the results are almost identical on the two finer grids (Grid II and Grid III). From theses results, it is demonstrated that both Grid II and Grid III are valid for resolving all essential features of the flow. In this study, all results of calculation were shown on Grid III even though Grid II was sufficient to resolve all essential features of the flow.

Note that all the forces for different diameter ratios, Da/Dp (ratio of the aneurysm neck to the diameter of the parent

vessel), were computed from the same flow field by varying the area of the virtual coil. Fig. 13 shows the variation of the force during the pulsatile cycle for several values of diameter ratio. The force varies substantially during the cycle and is affected by the diameter ratio. In Fig. 14, the maximum value of the force during the cycle is shown as a function of diameter ratio. For the parameters considered, maximum force impinging on an aneurysm neck having the same diameter as
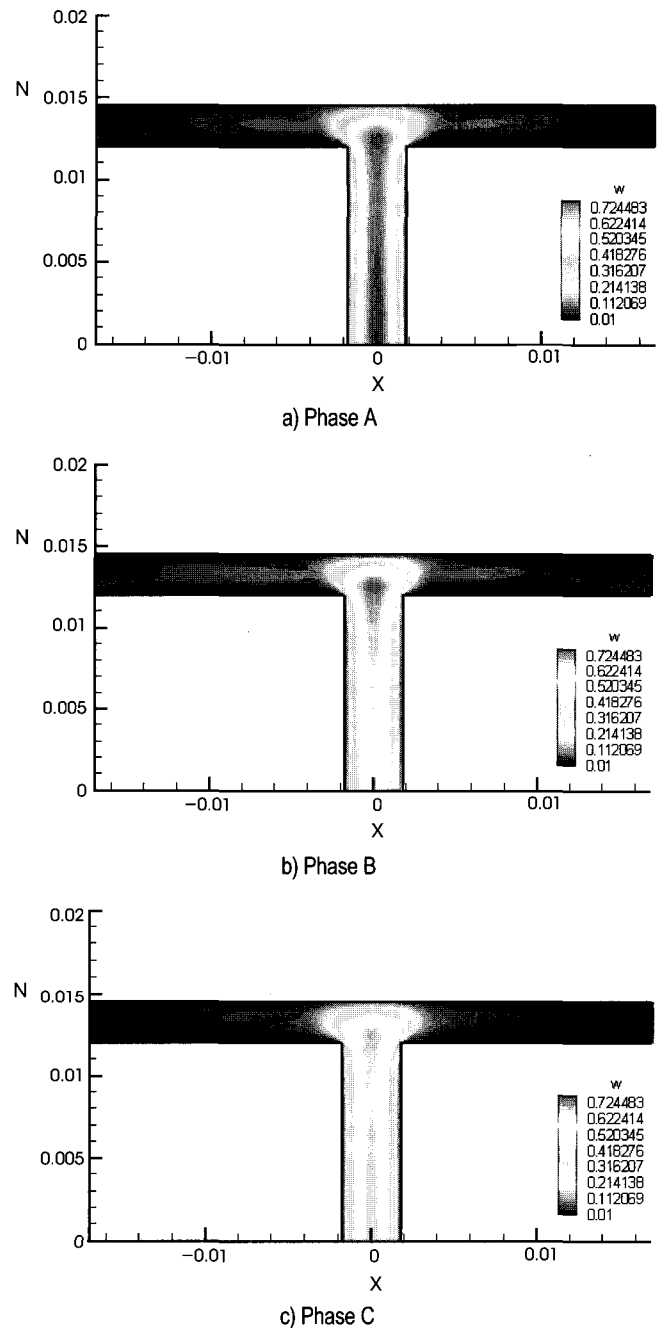
Fig. 11. Contours of velocity in the direction perpendicular to the aneurysm neck.
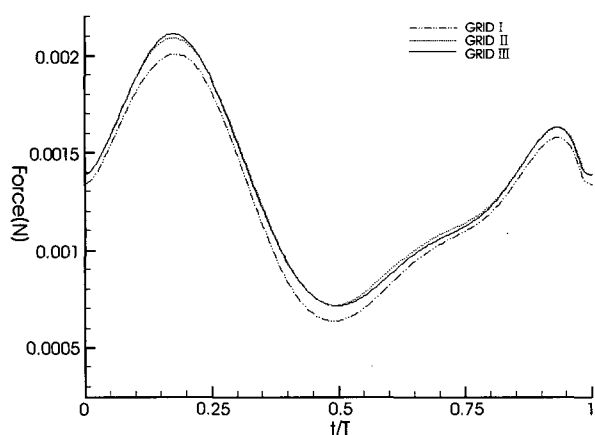
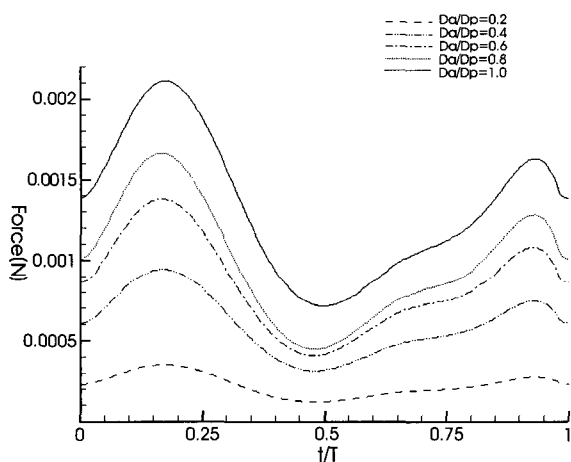Fig. 12. Comparison of force on aneurysm neck for three different levels of mesh refinement. (Da = Dp)

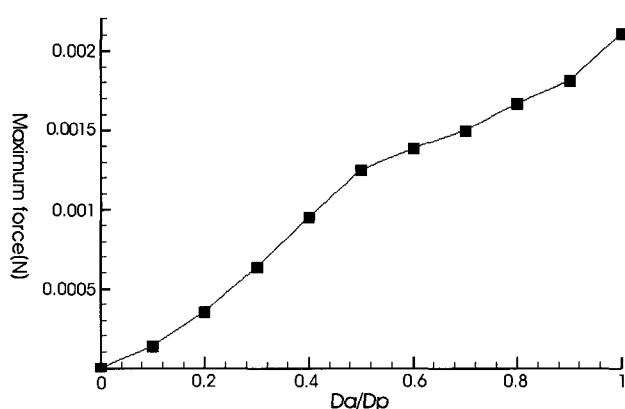Fig. 13. The variations of the force on the aneurysm neck during a flow cycle.

Fig. 14. The maximum force on the neck during a flow cycle.

the parent artery is found to be approximately 0.00211 N. The present results are qualitatively similar to the ones reported in
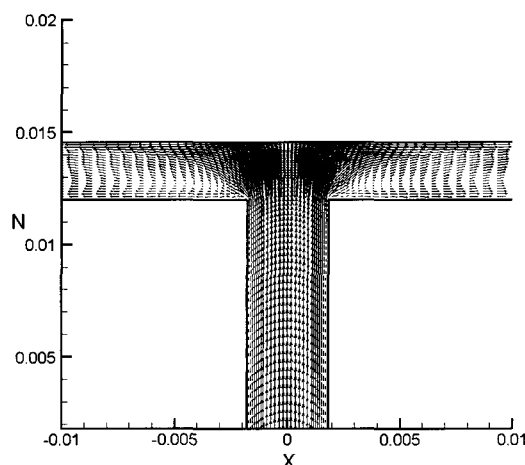

Fig. 15. Velocity vectors near the aneurysm neck at the peak flow rate.

Lieber's calculation [15] where a simplified control volume approach was used. The maximum force however is approximately 21% lower than that of Lieber's results. This is expected since the details of the flow near the stagnation point (see Fig. 15), which have a large effect on the forces, are properly captured in the present computations.

IV. CONCLUSION

I n this study, a methodology to assess the force experienced by a coil mass at the aneurysm neck has been described. The forces exerted on the coils in an idealized aneurysm neck were computed by using a finite volume method for the non-Newtonian, incompressible, laminar flow. It is noted that the hemodynamic forces exerted by direct and repeated impingement of the pulsatile blood flow on the coiled aneurysm neck are larger for wide necked aneurysms and may be responsible for their compaction and aneurysm recanalization.

In clinical cases, flow regimes and geometries are more complex. These calculations, however, were limited to an idealized aneurysm model. For more accurate prediction of hemodynamic characteristics which include flow patterns, pressure, shear stress and blood jet impingement, it is required to consider more clinically relevant factors. Ongoing and future work will be focused on these issues.

REFERENCES

[1]   G.N. Foutrakis, H. Yonas, and R.J.Sclabassi, 1999, "Saccular aneurysm formation in curved and bifurcation arteries," *AJNR*, vol. 20, pp. 1309-1317, 1999.

[2]   B. Weir, "Unruptured intracranial aneurysms: a review," *J. Neurosurg.*, vol. 96, pp. 3-42, 2002.

[3]   M. R. Mayberg, H. H. Batjer, and R. Darcey, "Guidelines for the

management of aneurismal subarachnoid hemorrhage," *Circulation,* vol. 90, pp. 2592-2605, 1994.

[4] W. I. Schievink, "Intracranial aneurysms," *N. Engl. J. Med.,* vol.336, pp. 2840. 1997.

[5] A. J. Ringer, D. K. Lopes, A. L. Boulos, L. R. Guterman, and L. N. Hopkins, "Current techniques for endovascular treatment of intracranial aneurysms," *Sem. Cerebrovasc. Diseases Stroke,* vol. 1, 2001.

[6] International Study of Unruptured Intracranial Aneurysms Investigators (The ISUIA Group), "Unruptured intracranial aneurysms: natural history, clinical outcome, and risks of surgical and endovascular treatment," *Lancet,* vol. 362, pp. 103-110, 2003.

[7] International Subarachnoid Aneurysms Trial (ISAT) Collaborative Group, "International Subarachnoid Aneurysms Trial (ISAT) of neurosergical clipping versus endovascular coiling in 2143 patients with ruptured intracranial aneurysms: a randomized trial," *Lancet,* vol. 360, pp. 1267-1274, 2002.

[8] J. Thornton, G. M. Debrun, V. A. Aletich, Q. Bashir, F. T. Charbel, and J. Ausman, "Follow-up angiography of intracranial aneurysms treated with endovascular placement of Guglielmi detachable coils," *Neurosurgery,* vol. 50, pp. 239-249, 2002.

[9] A. Fernandez Zubillaga, G. Guglielmi, F. Vinuela, and G. R. Duckwiler, "Endovascular occlusion of intracranial aneurysms with electrically detachable coils: correlation of aneurysm neck size and treatment results," *AJNR,* vol. 15, pp. 815-820, 1994.

[10] V. B. Graves, C. M. Strother, C. R. Partington, and A. Rappe, "Flow dynamics of lateral carotid artery aneurysms and their effects on coils and balloons: an experimental study in dogs," *AJNR,* vol. 13, pp. 189-196. 1992.

[11] Y. P. Gobin, J. L. Counord, P. Flaud, and J. Duffaux, "In vitro study of hemodynamics in a giant saccular aneurysm model: influence of flow dynamics in the parent vessel and effects of coil embolization," *Neuroradiology,* vol. 36, pp. 530-536. 1994.

[12] C. Groden, J. Laudan, S. Gatchell, and H. Zeumer, "Three dimensional pulsatile flow simulation before and after endovascular coil embolization of a terminal cerebral aneurysm," *J. Cereb.*

Blood Flow Metab., vol. 21, pp. 1464-71, 2001.

[13] B. B. Lieber, and M. J. Gounis, "The physics of endoluminal stenting in the treatment of cerebrovascular aneurysms," *Neurol. Res.,* vol. 24, suppl. 1, pp. S33-42, 2002.

[14] Jou Liang-Der, M. Q. Christopher, L. Y. William, T. L. Michael, H. Randall, M. Alastair and S. David, "Computational approach to quantifying hemodynamic forces in giant cerebral aneurysms," *AJNR Am J Neuroradiol,* vol.24, pp. 1804-1810, 2003.

[15] B.B. Lieber, C. Sadasivan, M.J.Gounis, and A.K.Wakhloo, "The role of blood impulse in the cerebral aneurysm coil compaction: effect of aneurysm neck size," in *Proc. IMECE '03, Washington D.C.,* Nov. 2003, pp.16-21.

[16] H. S. Byun, and K.Rhee, "CFD modeling of blood flow following coil embolization of aneurysms," *Medical Engineering Physics,* 2004.

[17] Gordan, R. Stuhne and A. David, "Finite-element modeling of the hemodynamics of stented aneurysms," *J. Biomech. Eng.,* vol. 126, pp. 382-387, 2004.

[18] R.B. Bird, R.C. Armstrong, and O. Hassager, *Dynamics of Polymer Liquids,* second ed., vol. 1, New York: Wiley, 1987.

[19] M. Ojha, S. C. Richard, K. Cobbold, Wayne Johnston and Richard L. Hummel, "Pulsatile flow through constricted tubes: an experimental investigation using photochromic tracer methods," *J. Fluid Mech.,* vol. 203, pp. 173-197, 1989.

[20] A. Hernan, and Gonzalez, "On prediction incompressible flows by using a stabilized finite difference method with penalty," *Applied Mathematics and Computation,* vol. 156, pp. 439-454m, 2004.

[21] S.Einav, H. J. Berman, R. L. Fuhro, S. P. R. Di Giovanni, and J. D. Fridman, "Measurement of velocity profiles or red blood cells in the microcirculation by laser Doppler anemometry (LDA)," *Biorheology,* vol. 12, pp. 207-210, 1975.

[22] D. R. Enzmann, M. R. Ross, M. P. Marks, and N. J. Pelc, "Blood flow in major cerebral arteries measured by phase-contrast cine MR," *AJNR: American Journal of Neuroradiology,* vol. 15, pp.123-129, 1994.